Development of tungsten doped Ni-Zn nano-ferrites with fast response and recovery time for hydrogen gas sensing application

A. Pathania, P. Thakur, A.V. Trukhanov, S.V. Trukhanov, L.V. Panina, U. Luders, A. Thakur

Results in Physics 15 (2019) 102531

Contents lists available at ScienceDirect

Results in Physics

journal homepage: www.elsevier.com/locate/rinp

Development of tungsten doped Ni-Zn nano-ferrites with fast response and recovery time for hydrogen gas sensing application

Abhilash Pathania[a], Preeti Thakur[b], Alex V. Trukhanov[c,d], Sergei V. Trukhanov[c,d], Larissa V. Panina[c], Ulrike Lüders[e], Atul Thakur[f]

[a] Shoolini University of Biotechnology and Management Sciences, Post Box 9, Solan, HP 173 212, India
[b] Department of Physics, Amity School of Applied Sciences, Amity University Haryana, Gurgaon 122413, India
[c] National University of Science and Technology, MISIS, Moscow 119991, Russia
[d] SSPA "Scientific and Practical Materials Research Centre of NAS of Belarus", 220072, Minsk, P. Brovki str., 19, Belarus
[e] Laboratoire de Cristallographie et Sciences des Matériaux CRISMAT, Caen, France
[f] Centre of Nanotechnology, Amity University Haryana, Gurgaon 122413, India

ARTICLE INFO

Keywords:
Co-precipitation
Pellet type resistive sensor
Platinum decomposition
Hydrogen gas sensor
High selectivity
Low temperature
Sensitivity

ABSTRACT

This paper reports on the study of series of tungsten doped $Ni_{0.5}Zn_{0.5}W_xFe_{2-x}O_4$ (x = 0.0, 0.2, 0.4, 0.6, 0.8, 1.0) ferrites synthesized by a co-precipitation scheme. The crystallite size varies from 62 to 49 nm and the scanning electron microscope (SEM) images show the spinel cubic structure of the powder sample. Energy Dispersive X-ray Fluorescence Spectroscopy (EDXRF) confirms the presence of Ni, Zn, W and Fe elements in the prepared samples. The specific surface areas of the $Ni_{0.5}Zn_{0.5}W_{0.2}Fe_{1.8}O_4$, $Ni_{0.5}Zn_{0.5}W_{0.4}Fe_{1.6}O_4$ and $Ni_{0.5}Zn_{0.5}W_{0.6}Fe_{1.4}O_4$ samples calculated from Brunauer-Emmett-Teller (BET) method are 18.9 m^2/g, 21.5 m^2/g and 24.6 m^2/g, respectively. The metal oxide pellet type resistive sensor was made for gas sensor application. These sensors are selective for hydrogen (H_2) gas. The performance of these sensors for sensing hydrogen gas at a concentration of 1000 ppm in the temperature range 80–300 °C has been investigated. Platinum electrodes were deposited on all the pellets by RF sputtering technique. The subsequent decomposition of platinum oxides on the metal oxide pellet surface results in an increase in surface roughness and electrical resistivity. The sensor shows a change in resistance from $1.21 \times 10^5\ \Omega$ to $7.83 \times 10^4\ \Omega$ in the presence of H_2 gas even at alow temperature. The composition with x = 0.2 at an optimum temperature of 180 °C showed a fast response (14 s) and recovery time (20 s). High sensitivity, low cost, long term stability, high selectivity and fast response at low temperature makes this sensor useful for industrial applications.

Introduction

The demand for energy is increasing with the rapid expansion of automobile and other industrial sectors. Fuel consumption leads to pollution. Hydrogen is a clean source of energy with high energy density, so it has the potential to be the future source of fuel with wide applications in aircraft, chemical processes, fuel cells, nuclear, medical, petrochemical, transportation, coal mines, thermal power stations etc. [1–4]. Hydrogen gas is odorless, colorless and tasteless. Hydrogen can easily leak out due to its a low molecular weight and may cause fires or explosions at a concentration greater than 4% in dry air [5–7]. Hydrogen gas can't be detected by human beings. The detection of hydrogen gas in ppm scale is necessary as it is highly flammable. Hydrogen detection techniques can be classified as chemoresistors, diodes and transistors, mechanical, optical, catalytic, and acoustic gas sensors [8–13]. Chemoresistive sensors are more significant because of low synthesis cost, high stability, high sensitivity, selectivity, electrical responses to different gases [14,15]. The sensor's performance depend on the composition of materials, crystallite size, porosity and exposed surface area, etc. [16,17]. The mesoporous structure (pores diameter between 2 and 200 nm) is mostly preferred for the gas sensor application [18]. Ferrites with nanosized and lower density structures are preferred for gas sensors. Nanosized grains are preferred to increase the specific surface area for the analyte gas [19]. Nanoferrites can be synthesised by any of the methods like solid-state reaction method, sol–gel auto-combustion, hydrothermal, reverse-micelle method, or chemical co-precipitation method [20–22]. Chemical co-precipitation is a significant technique because it gives fine particle size, uniform chemical composition and better physical properties.

Ni-Zn, a multifunctional semiconductor material is one of the most studied metal oxides due to its remarkable electrical and electronic properties [23]. Gas-sensing properties of Ni-Zn ferrite has been studied by many researchers [24]. Dalawai et al. prepared Ni–Zn ferrite thick film gas sensors and found that $Ni_{0.6}Zn_{0.4}Fe_2O_4$ is more sensitive for Cl_2 followed by ethanol as compared to LPG [25].

Transition-metal oxides, like SnO_2, ZnO, FeO, Ga_2O_3, Fe_2O_3, TiO_2,

https://doi.org/10.1016/j.rinp.2019.102531
Received 10 April 2019; Received in revised form 18 July 2019; Accepted 20 July 2019
Available online 25 July 2019

In_2O_3, MoO_3, and WO_3, show a huge variation in their electrical resistance in the presence of gas [26–30]. WO_3 doping with water produces a porous sensor material, which improves sensitivity and response time characteristics [31]. Pure WO_3 can sense oxidizing gases such as NO, O_3, and Cl_2; but for reducing gases, noble catalysts (Pt, Au, and Pd) are required for the surface modification [32]. The effect of noble catalysts on the metal oxide surface for gas sensing properties has been broadly studied by many researchers [33,34]. Various methods have been applied for the deposition of noble catalysts, namely, sputtering, pulsed laser deposition, ferrite plating, dip coating process, spray pyrolysis, and electrodeposition [35–40]. High operating temperature becomes the bottleneck for resistive-type semiconductor material for its applications in the field of gas sensor. Therefore, worldwide researchers are trying to improve this bottleneck by means of multiple methods.

In the present work, our focus was to develop the nanoferrites for a gas sensor application with high sensitivity at low power consumption. Therefore, tungsten doped Ni-Zn nanoferrite pellet type resistive sensor is prepared for hydrogen gas and tested at a temperature range from 80 °C to 300 °C at 1000 ppm. The Zn is more volatile and is loss from ferrite above 1000 °C The gas sensing properties of different compositions of tungsten doped Ni-Zn ferrites with platinum coating is well explained in this paper.

Experimental procedure

A chemical co-precipitation method was used to synthesise a series of metal oxide with chemical formula $Ni_{0.5}Zn_{0.5}W_xFe_{2-x}O_4$ where $0 \leq x1.0$ in steps of 0.2. Nickel chloride hexahydrate, zinc chloride, tungsten trioxide and iron (III) chloride hexahydrate chemicals of high purity (99.9%) were used to synthesize this series. The experimental detail along with the structural, optical, electrical and mechanical properties of this series is already explained in our previous work [41].

Fabrication of pellet sensor

The powdered samples after pre-sintering at 850 °C for three hours were allowed to cool to room temperature and were crushed into uniform and fine powder with the help of a mortar and pestle. 5 g of an organic binder poly vinyl alcohol (PVA) was mixed with 10 ml of distilled water in order to make a homogenous solution. Then 0.05 ml of this solution of PVA was missed with a quantity of 0.3 g powdered sample and crushed to fine powder again. The pellet of diameter 10 mm was made under a pressure of 10 tonne by using uniaxial hydraulic press. These pellets so prepared were finally subjected to sintering at a temperature of 1000 °C for another 3 h for densification and removal of organic binder. For the gas sensing measurements, Platinum electrodes about 100 nm thick and 500 μm wide were deposited on all the pellets by RF sputtering technique using shadow mask. In the presence of gas comprising 50% Ar and 50% O_2, 30 W fixed RF power was applied to the target in the chamber at a pressure of 3×10^{-6} Torr.

Experimental set-up for gas sensing test

Fig. 1 shows the schematic diagram of gas sensing equipment. A tailor made gas calibration chamber was used for gas sensing which is attached with a rotary pump (for vacuum in the testing chamber), heating assembly, 2 probe system (pure Gold electrodes) for the resistance measurements, needle valves for injecting the calibrated quantity of gas. The Keithley 6514 electrometer was used to record the value of resistance during the entire sensing cycle for each sensor.

Gas sensing mechanism

The oxide sensors show significant variation in the electrical resistance because of the reversible interaction of the gas with the pre-adsorbed ambient oxygen [42]. Metal oxide based gas sensors generally give better response at a high temperature. When the sensor is heated in air, oxygen ions (O_2^-, $O^{2-}O^-$) first chemisorbed on the metal oxide sensor surface, chemisorption of oxygen electrons leads to formation of a depleted layer. This layer act as a potential barrier for electron migration and increases the sensor surface resistance [43]. The reaction on the sensor surface is as follows

$$O_{2(g)} + e^- \leftrightarrow O^-_{2(ads)} \quad (1)$$

$$O^-_{2(ads)} + e^- \leftrightarrow 2O^-_{(ads)} \quad (2)$$

$$O^-_{(ads)} + e^- \leftrightarrow O^{-2}_{(ads)} \quad (3)$$

The Eqs. (1)–(3) show that oxygen may be chemisorbed on the sensor surface. This absorbed oxygen roots the electron depletion, which increases the sensor resistance, whereas, the reducing gas (R_g) is absorbed on sensor surface as follows

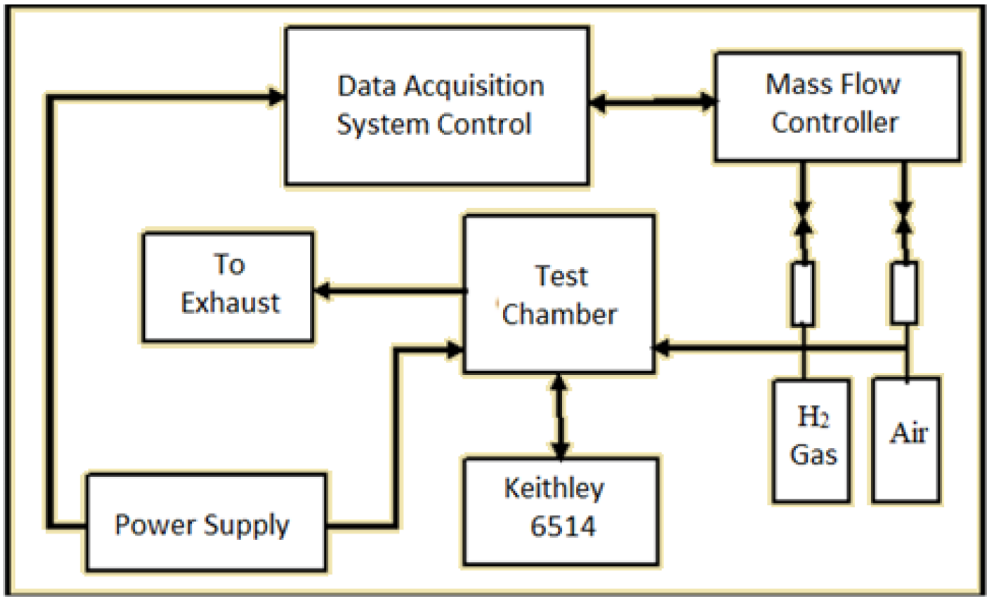

Fig. 1. The schematic diagram of gas sensing equipment.

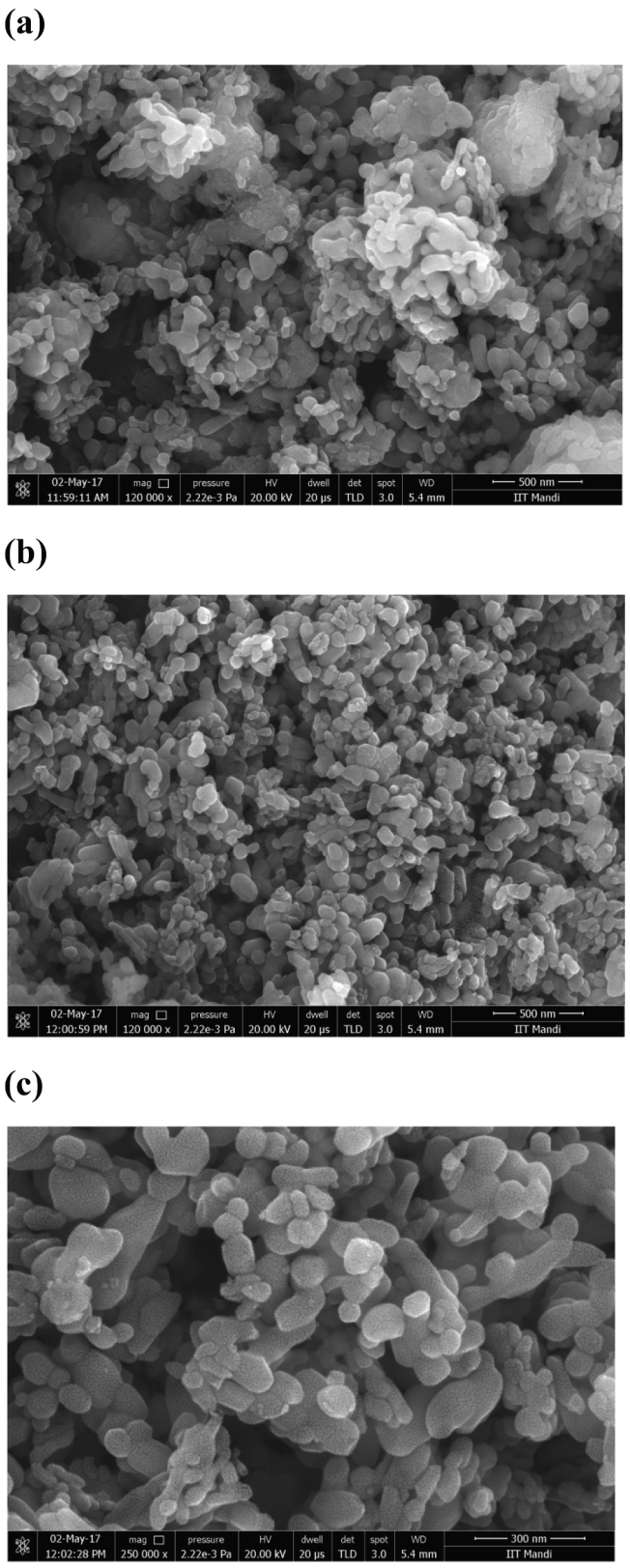

Fig. 2. The SEM image of the powder samples for the compositions (a) $Ni_{0.5}Zn_{0.5}Fe_2O_4$, b) $Ni_{0.5}Zn_{0.5}W_{0.4}Fe_{1.6}O_4$, &(c) $Ni_{0.5}Zn_{0.5}W_{0.8}Fe_{1.2}O_4$.

$$R_g(ads) + O^-(ads)_{RgO} \leftrightarrow (ads) + e^- \quad (4)$$

$$R_g(ads) + O^{2-}(ads) \leftrightarrow_{RgO} (ads) + 2e^- \quad (5)$$

At a normal temperature, the sensor surface adsorbed oxygen. The adsorbed oxygen starts to desorb with an increase in temperature. When reducing (R_g) gas is introduced, it reacts with the chemisorbed oxygen on the surface and released electrons to the conduction band of the sensor. This causes a decrease in the electrical resistance. The electrical resistance variation determines the response of a sensor. Therefore, for every sensor there must be some optimum temperature where the gas response is maximized. The sensor response for reducing gas is calculated by using eq. (6).

$$S = \frac{R_a}{R_g} - 1 \quad (6)$$

whereR_a and R_g are the resistance of sensing element in the presence of the air and target gas respectively.

Role of noble metal for gas sensor

Noble metals (Pd, Pt), reduces the adsorption activation energy and hence improves the sensor performance. The noble metals increase the reaction rate by increasing the target gas concentration on the surface of the sensor. It also provides a reaction pathway and enhances sensitivity, selectivity and reliability [44,45]. The noble metals (−ve) are having low Fermi level as compare to the metal oxides (+ve) used for the sensors. So there is a rapid exchange of electrons until the Fermi level of both the metals become equal. Schottky barrier is formed at the interface, which prevents the recombination of electron-hole pairs and improves the performance of the sensor [46,47].

Results & discussion

The crystallite size and porosity are important factors for the metal oxide gas sensors. The crystallite size, lattice parameter, density and porosity of the tungsten doped Ni-Zn series prepared by a co-precipitation method was calculated and explained by using X-ray diffraction data and reported in our earlier work [41]. The crystallite size was found in the range from 62 to 49 nm. The morphology and microstructures of the tungsten doped Ni-Zn ferrites series was studied by a scanning electron microscope. Fig. 2(a)–(c) shows the SEM images of the sintered powder samples for the compositions $Ni_{0.5}Zn_{0.5}W_xFe_{2-x}O_4$ (x = 0.0, 0.4, 0.8). SEM micrographs clearly show the aggregation or accumulation in the ferrite nanoparticles with an average grain size of about 55 nm.

To confirm the successful incorporation of the tungsten ion into the ferrite system and stoichiometric composition of the samples, the energy dispersive X-ray fluorescence spectroscopy was performed on Panalytical epsilon 4. Fig. 3 depicts the presence of all the desired elements (nickel, zinc, tungsten and iron) within the prepared samples except for the oxygen. This is due to the fact that for EDXRF measurement, the detector used for detection of characteristics X-rays of the elements is a peltier cooled Si (Li) detector, where the element below Na (here oxygen) cannot be detected as the characteristic X-ray from this elements gets absorbed by the detector window. Table 1 shows atomic mass percentage values of the respective elements in the concerned samples as determined from the EDXRF spectral analysis. The results ruled out the possibilities of inhomogeneous distribution of tungsten ions into the system and also supports that the precursors have undergone chemical reaction in the preferred stoichiometric ratio.

The BET analysis was measured by nitrogen sorption using ASAP 2010 and analyzed based on Brunauer-Emmett-Teller theory. To investigate the specific surface and pore size distribution of the ferrite samples after annealing at 1000 °C, nitrogen gas adsorption–desorption measurement was performed. As shown in Fig. 4(a, c and e), all the curves displayed IV-type sorption isotherms with obvious loops, which demonstrates that the annealed $Ni_{0.5}Zn_{0.5}W_xFe_{2-x}O_4$ (x = 0.2, 0.4, and 0.6) samples were mesoporous materials. The specific surface areas of the $Ni_{0.5}Zn_{0.5}W_{0.2}Fe_{1.8}O_4$, $Ni_{0.5}Zn_{0.5}W_{0.4}Fe_{1.6}O_4$ and $Ni_{0.5}Zn_{0.5}W_{0.6}Fe_{1.4}O_4$ foams calculated from Brunauer-Emmett-Teller

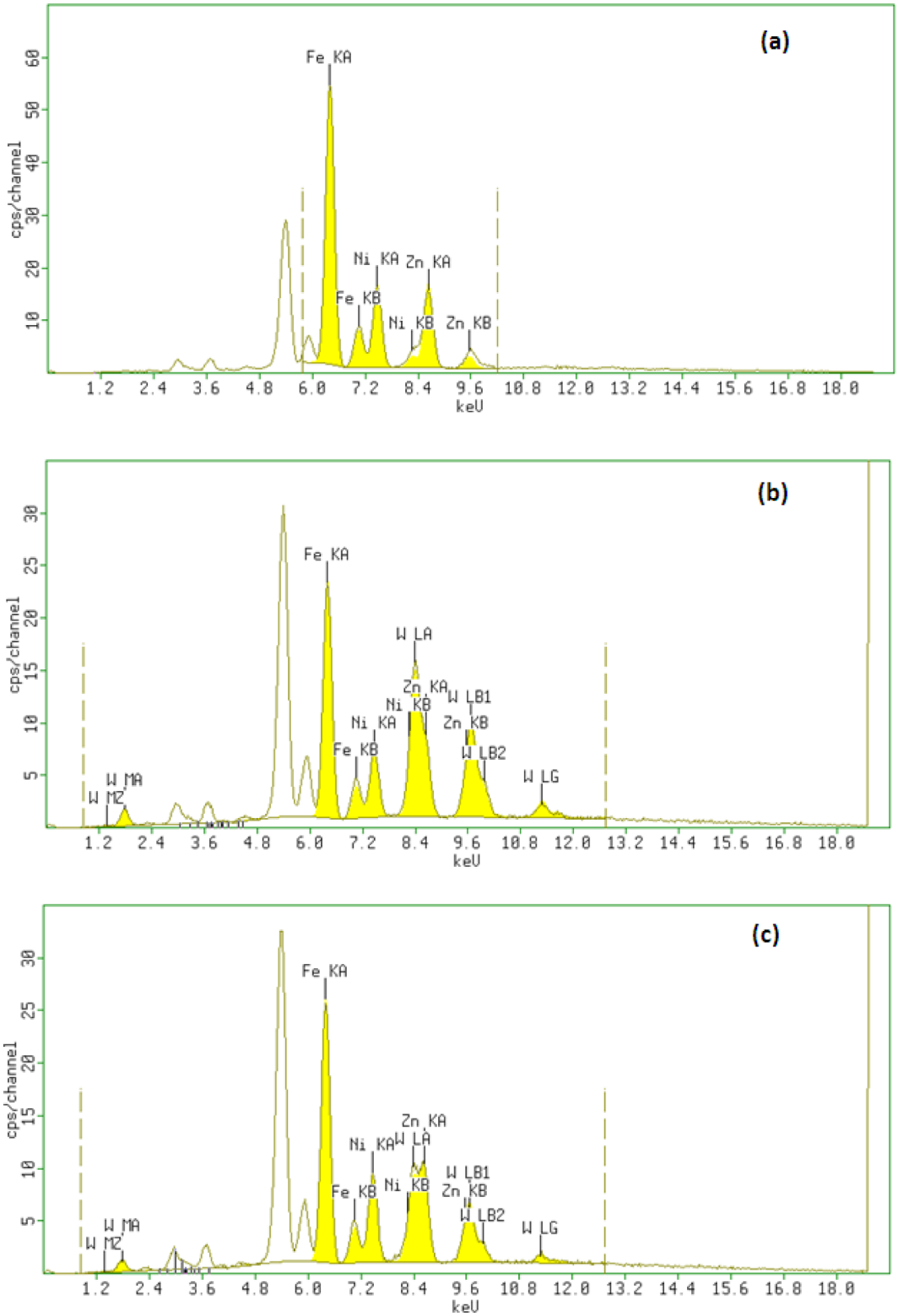

Fig. 3. Depicts the XRF spectral of (a) $Ni_{0.5}Zn_{0.5}Fe_2O_4$, (b) $Ni_{0.5}Zn_{0.5}W_{0.2}Fe_{1.8}O_4$, (c) $Ni_{0.5}Zn_{0.5}W_{0.4}Fe_{1.6}O_4$, (d) $Ni_{0.5}Zn_{0.5}W_{0.6}Fe_{1.4}O_4$, (e) $Ni_{0.5}Zn_{0.5}W_{0.8}Fe_{1.2}O_4$, (f) $Ni_{0.5}Zn_{0.5}W_{1\cdot0}Fe_{1.0}O_4$,

(BET) method are 18.9 m^2/g, 21.5 m^2/g and 24.6 m^2/g, respectively. From Fig. 4, the pore size distribution diagrams of the annealed samples show a multi-peak coexistence with one dominant peak centered about 2–3 nm. The larger the pore size, the smaller the number of pores. It also can be proved to be a hierarchical porous structure with lots of mesopores on the surface of the layered structure, which is in agreement with the SEM analysis. These results further indicate that a higher specific surface area can be obtained in the samples that have a low mass density.

Before starting the gas sensor measurements, all the sensors were kept at 350 °C in dry air (79% Nitrogen & 21% Oxygen) for 3 h, to study their microstructure. The chamber for gas testing was evacuated by a

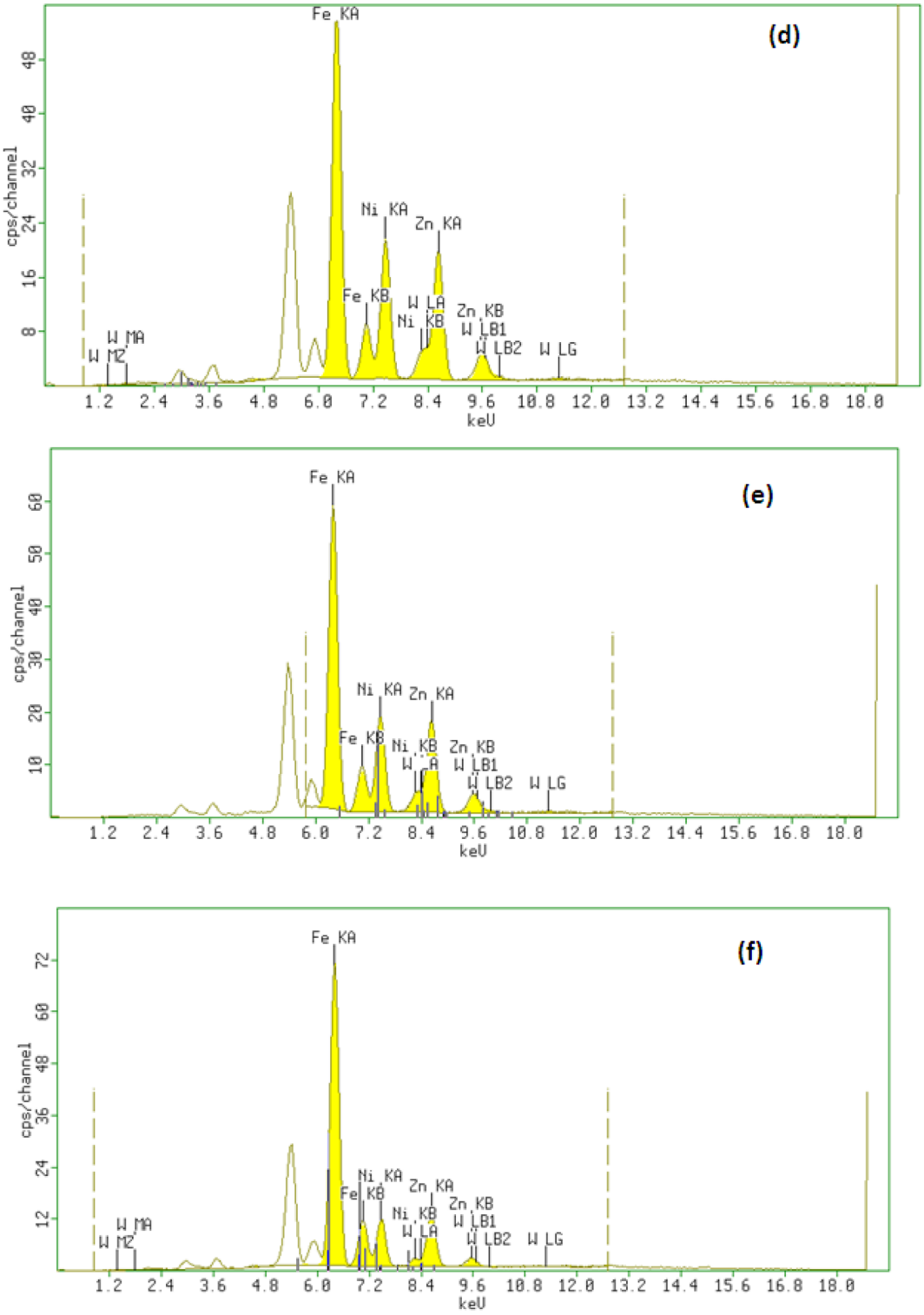

Fig. 3. (*continued*)

rotary pump at a pressure of approximately 10^{-2} Torr. Initially, the dry air is allowed to enter the air tight chamber until the resistance value is stabilized. Then the dry air along with requisite concentration of hydrogen (H_2) gas was introduced into the calibration chamber. The electrometer (Keithley 6514) was used to record the value of resistance of all the sensors during the entire sensing cycle. The resistance of the sensors was in the range of $1.21 \times 10^5\,\Omega$–$7.83 \times 10^4\,\Omega$ under dry air atmosphere at a temperature from 80 to 300 °C. The same process was repeated for all the sensors.

Response characteristics

Fig. 5 shows the sensitivity of all the pellet sensors in the temperature range from 80 to 300 °C at 1000 ppm of H_2 gas. With the rise in temperature the kinetic energy of the atoms increases due to which adsorption of atoms on reactive sites increases and found to be optimum for temperature 180–200 °C. With further increase in temperature the Brownian motion of the atoms dominates and hence sensitivity decreases. Whereas, no sensitivity is noticed when concentration of

Table 1
Atomic mass percentage data obtained from XRF analysis of the samples.

	Ni (%)	Zn (%)	W (%)	Fe (%)
$Ni_{0.5}Zn_{0.5}Fe_2O_4$	16.7	16.5	–	66.6
$Ni_{0.5}Zn_{0.5}W_{0.2}Fe_{1.8}O_4$	16.2	16.7	7.1	58.1
$Ni_{0.5}Zn_{0.5}W_{0.4}Fe_{1.6}O_4$	16.5	17.8	15.4	49.4
$Ni_{0.5}Zn_{0.5}W_{0.6}Fe_{1.4}O_4$	15.8	16.9	22.8	44.6
$Ni_{0.5}Zn_{0.5}W_{0.8}Fe_{1.2}O_4$	16.2	16.6	28.7	37.6
$Ni_{0.5}Zn_{0.5}W_{1.0}Fe_{1.0}O_4$	15.9	16.1	33.6	34.3

tungsten in the matrix is nil. With a slight addition of tungsten (x = 0.2) he sensitivity is found to be noticeable, with further increase in concentration of tungsten, the overall sensitivity is very minute. All tungsten doped sensors show a higher response at a temperature of 180 °C. This confirms that 180 °C is the optimum temperature where maximum response of 60.97% is achieved for hydrogen gas at 1000 ppm. After that the response is found to decrease continuously due to the low-degree of reaction between chemisorbed oxygen and hydrogen, the response of the sensors is less below 180 °C. However, above 180 °C, there is again a drop in the response because of the fast degree reaction between chemisorbed oxygen and hydrogen gas which limited the effective diffusion and adsorption of hydrogen on the surface of the sensor [48]. The sensor with tungsten concentration (x = 0.2) shows the highest response as compared to other sensors. Fig. 6 shows the response of the sensor with tungsten (x = 0.2) at an operating temperature of 180 °C for different concentrations 850, 900, 950 and 1000 ppm of hydrogen gas. It is clearly observed that response of the gas increases with an increase in the concentration of the gas molecules on the grain surface [49]. This is due to the fact that the oxygen chemisorption capacity increases with greater amount of Fe^{2+}. However, if the Fe^{2+} concentration is too high then the Debye width is narrower, and the gas response of the sensor is reduced. As the concentration of tungsten increases, the iron content decreases which also decreases the amount of $Fe^{2+}$and hence, response increases [24].

Fig. 7 shows the change in resistance with time at a temperature of 180 °C in the presence of 1000 ppm hydrogen gas. The 1000 ppm of hydrogen gas is injected at different times and it shows the same behaviour for all times.

Response & recovery time

Response and recovery time are two important parameters for a gas sensor. Fig. 8 shows the response time for all the tungsten doped sensors in the temperature range 80–300 °C in the step of 20 °C for 1000 ppm of hydrogen concentration. The response time shows an increasing trend with an increase in tungsten doping for all the temperatures. This may be due to the porosity. Large pores lead to faster reaction as compared to small pores. The response time for all the sensors is found to decrease due to the fast reaction with an increase in temperature. Since the sensor with tungsten (x = 0.2) shows the higher sensitivity, so the resistance variation in the presence of H_2 gas was recorded for 8 weeks in

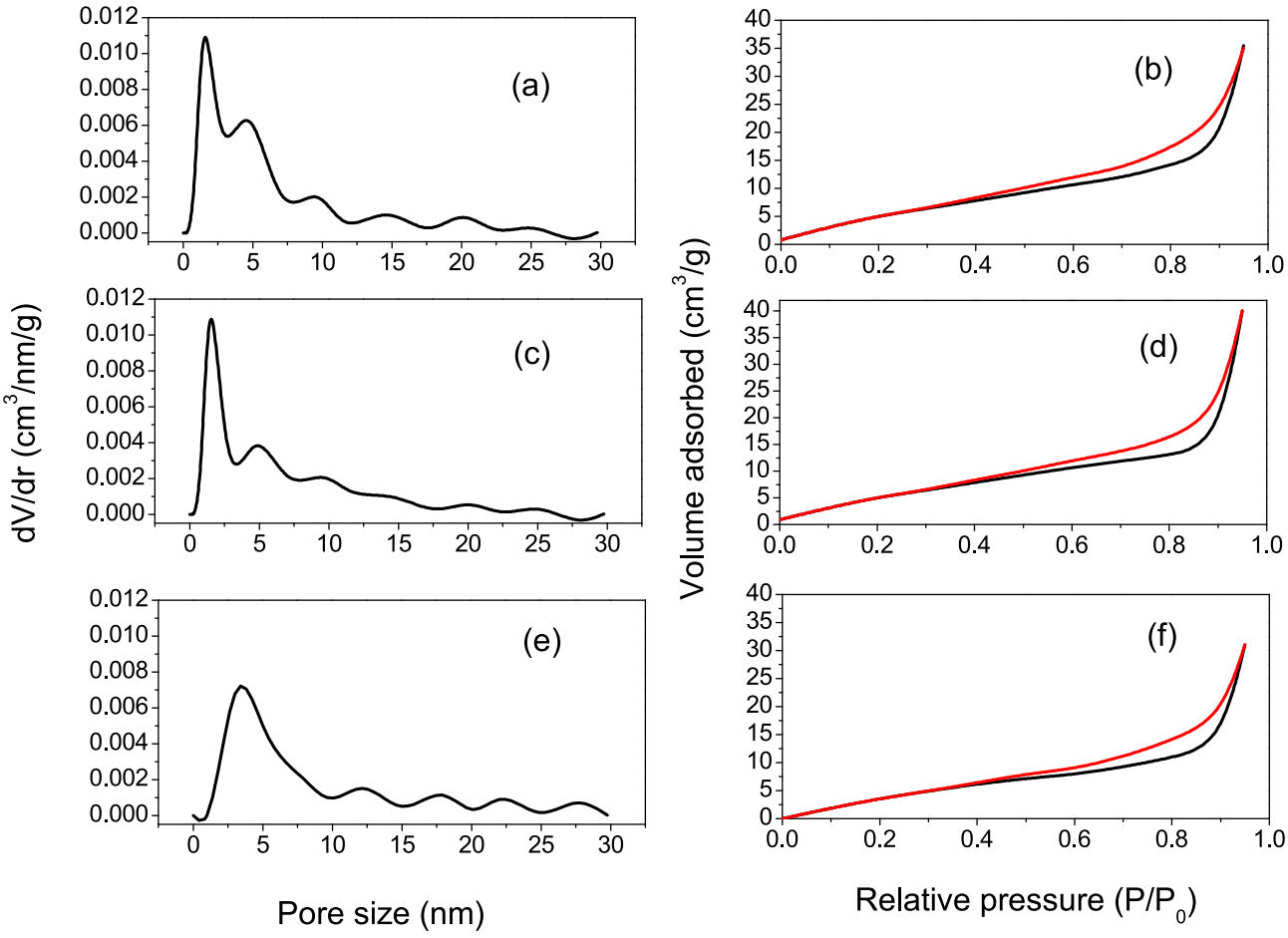

Fig. 4. The N2 adsorption–desorption isotherm and pore size distribution of the samples annealed at 1000 °C (a, b) $Ni_{0.5}Zn_{0.5}W_{0.2}Fe_{1.8}O_4$, (c, d) $Ni_{0.5}Zn_{0.5}W_{0.4}Fe_{1.6}O_4$, and (e, f) $Ni_{0.5}Zn_{0.5}W_{0.6}Fe_{1.4}O_4$.

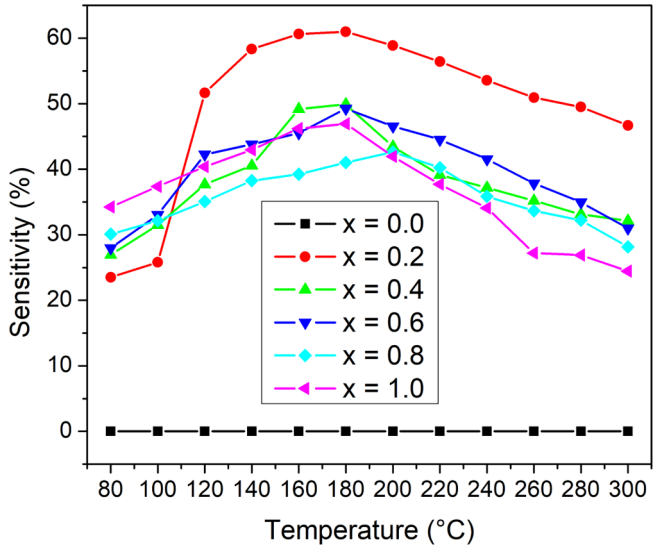

Fig. 5. Sensitivity (%) the sensors with the temperature range from 80 to 300 °C at 1000 ppm of H_2concentration.

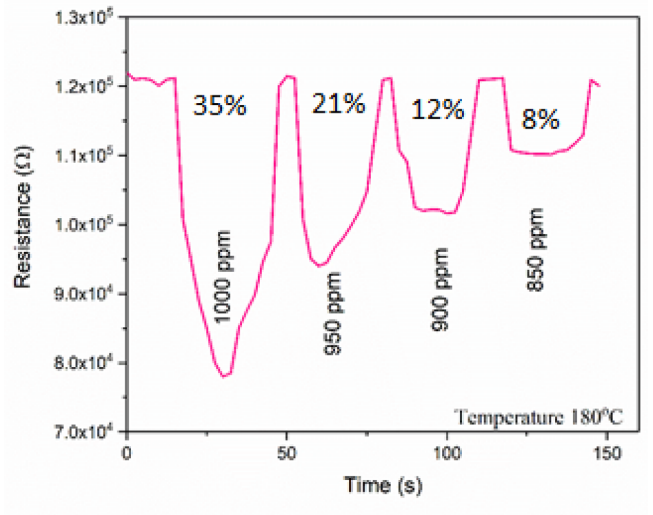

Fig. 6. The response of the sensor with tungsten (x = 0.2) at an optimum temperature of 180 °C for a concentration 850, 900, 950 and 1000 ppm of hydrogen gas.

the interval of one week at a temperature of 180 °C, which showed the same behaviour at all the times. Fig. 9 shows the stability of the sensor with tungsten (x = 0.2) i.e. changes in resistance with time in the presence of 1000 ppm hydrogen gas. Response & recovery time are the important parameters for the gas sensors. Fig. 10 shows the response time of all the sensors with respect to temperature from 80 to 300 °C. The recovery time for all the metal oxide gas sensors is more as compared to the response time [50,51]. Tungsten doped Ni-Zn ferrites with x = 0.2 at an optimum temperature of 180 °C showed a fast response (14 s) and recovery time (20 s).

Conclusion

A series of tungsten doped Ni-Zn (x = 0.0, 0.2, 0.4, 0.6, 0.8, 0.1) ferrite was synthesized by a co-precipitation method for gas sensor application. The crystallite size was in the range from 62 to 49 nm. The SEM images confirm the cubic spinel structure for all the samples. Platinum electrodes about 100 nm thick and 500 μm wide were deposited on all the pellets by RF sputtering technique. The parent sample

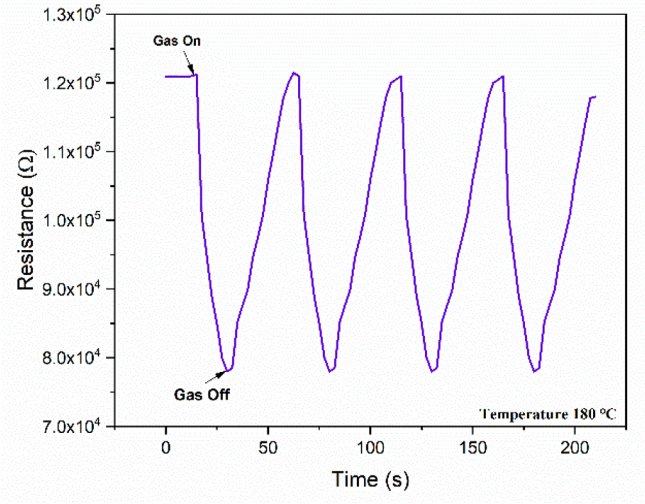

Fig. 7. The change in resistance with time at a temperature of 180 °C in the presence of 1000 ppm hydrogen gas.

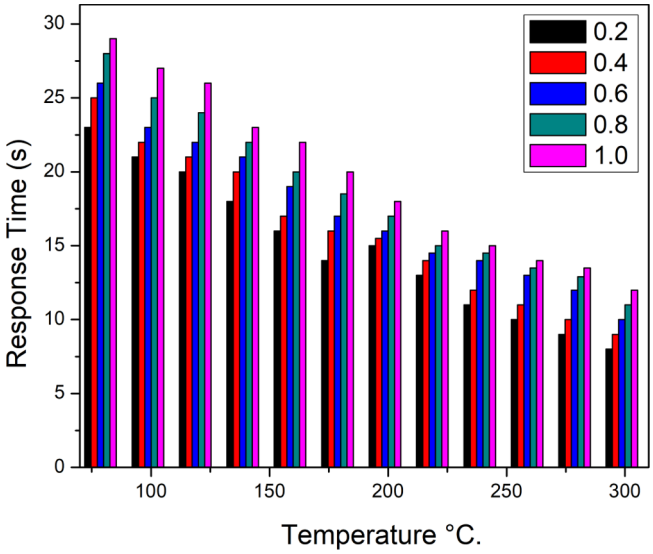

Fig. 8. The response time for all sensors at temperature range from 80 to 300 °C in a step of 20 °C.

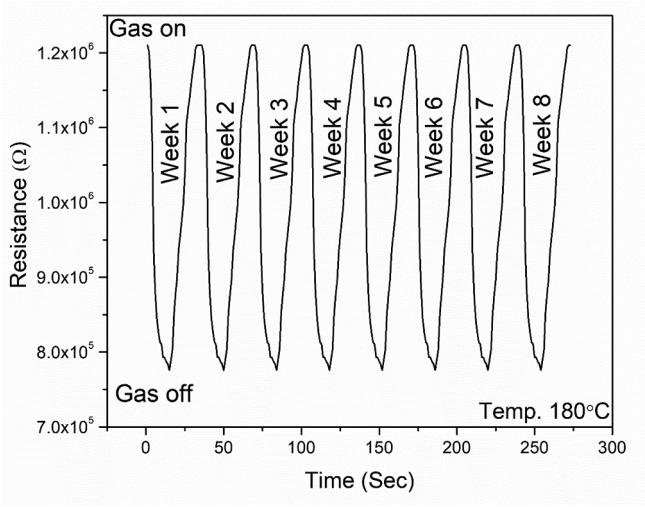

Fig. 9. Stability of the sensor with tungsten (x = 0.2).

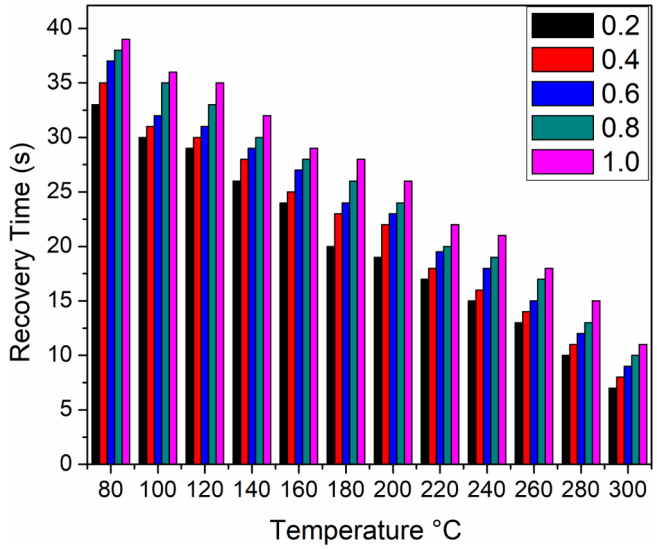

Fig. 10. The recovery time for all sensors at temperature range from 80 to 300 °C in a step of 20 °C.

without tungsten did not show any response to the hydrogen gas. The sensors with tungsten doping were very selective for hydrogen gas. All the samples were tested at a temperature range from 80 to 300 °C at a 1000 ppm of hydrogen gas. The sensor showed the change in resistance from $1.21 \times 10^5\ \Omega$ to $7.83 \times 10^4\ \Omega$ in the presence of H_2 gas even at a low temperature. All the sensors show a high response at an optimum temperature of 180 °C. The response and recovery time with temperature shows a decreasing trend. The sensor with tungsten concentration (x = 0.2) has been found to show the best results among all. A response of 60.97% at an optimum temperature of 180 °C; the response time and recovery time of 14 s and 20 s respectively. Low power consumption (180 °C) with fast response and recovery time make tungsten (x = 0.2) doped Ni-Zn ferrite sensor compatible for the industrial application for hydrogen gas sensing.

Acknowledgment

PT is grateful to the Department of Science and Technology (DST), Government of India, for the financial support vide sanction no SERB/F/7451/2013-14. This work was carried out with financial support in part from the Ministry of Science and Higher Education of the Russian Federation in the framework of Increase Competitiveness Program of NUST «MISiS» (grant No. P02-2017-2-4).

Appendix A. Supplementary data

Supplementary data to this article can be found online at https://doi.org/10.1016/j.rinp.2019.102531.

References

[1] Chaubey R, Sahu S, James OO, Maity S. A review on development of industrial processes and emerging techniques for production of hydrogen from renewable and sustainable sources. Renew Sustain Energy Rev 2013;23:443–62.
[2] Moriarty P, Honnery D. Hydrogen's role in an uncertain energy future. Int J Hydrogen Energy 2009;34:31–9.
[3] Momirlan M, Veziroglu TN. The properties of hydrogen as fuel tomorrow in sustainable energy system for a cleaner planet. Int J Hydrogen Energy 2005;30:795–802.
[4] Loloee R, Chorpening B, Beer S, Ghosh R. Hydrogen monitoring for power plant applications using SiC sensors. Sens Actuat B 2008;129:200–10.
[5] Zhang M, Zhen Y, Sun F, Xu C. Hydrothermally synthesized SnO_2 -graphene composites for H_2 sensing at low operating temperature. Mat Sci Eng B Adv. 2016;209:37–44.
[6] Haija M, Ayesh A, Ahmed S, Katsiotis M. Selective hydrogen gas sensor using $CuFe_2O_4$ nanoparticle based thin film. Appl Surf Sci 2016;369:443–7.
[7] Kim YK, Hwang S-H, Jeong SM, Son KY, Lim SK. Colorimetric hydrogen gas sensor based on PdO/metal oxides hybrid nanoparticles. Talanta 2018;188:356–64.
[8] Hsu CH, Chang CC, Tseng C-M, Chan C-C, Chao W-H, Wu Y-R, et al. An ultra-fast response gasochromic device for hydrogen gas detection. Sens Actuat B 2013;186:193–8.
[9] Kalanur SS, Yoo I-H, Lee Y-A, Seo H. Green deposition of Pd nanoparticles on WO_3 for optical, electronic and gasochromic hydrogen sensing applications. Sens Actuat B 2015;221:411–7.
[10] Sanger A, Kumar A, Chauhan S, Gautam YK, Chandra R. Fast and reversible hydrogen sensing properties of Pd/Mg thin film modified by hydrophobic porous silicon substrate. Sens Actuat B 2015;213:252–60.
[11] Anggraini SA, Breedon M, Miura N. Zn–Ta-based oxide as a hydrogen sensitive electrode material for zirconia-based electrochemical gas sensors. Sens Actuat B 2013;187:58–64.
[12] Gautam YK, Sanger A, Kumar A, Chandra R. A room temperature hydrogen sensor based on Pd–Mg alloy and multilayers prepared by magnetron sputtering. Int J Hydrogen Energy 2015;40:15549–55.
[13] Hübert T, Boon-Brett L, Black G, Banach U. Hydrogen sensors–A review. Sensors Actuat 2011;B157:329–52.
[14] Kim H-J, Lee JH. Highly sensitive and selective gas sensors using p-type oxide semiconductors. Sensors Actuat B 2014;192:607–27.
[15] Bogue R. Nanomaterials for gas sensing: a review of recent research. Sens Rev 2014;34:1–8.
[16] Wang C, Yin L, Zhang L, Xiang D, Gao R. Metal oxide gas sensors: sensitivity and influencing factors. Sensors (Basel, Switzerland) 2010;10:2088–106.
[17] Ma N, Suematsu K, Yuasa M, Shimanoe K. Pd size effect on the gas sensing properties of Pd-loaded SnO_2 in humid atmosphere. ACS Appl Mater Interfaces 2015;7:15618–25.
[18] Sakai G, Matsunaga N, Shimanoe K, Yamazoe N. Theory of gas-diffusion controlled sensitivity for thin film semiconductor gas sensor. Sens Actuat B 2001;80:125–31.
[19] Kapse VD, Ghosh SA, Raghuwanshi FC, Kapse SD. Nanocrystalline spinel $Ni_{0.6}Z_{n0.4}F_{e2}O4$: A novel material for $_H2S$ sensing. Mater Chem Phys 2009;113:638–44.
[20] Singh N, Agarwal A, Sanghi S, Singh P. Effect of magnesium substitution on dielectric and magnetic properties of Ni–Zn ferrite. Phys B 2011;406:687–92.
[21] Thakur A, Thakur P, Hsu J-H. Smart magneto dielectric nano-materials for the very high frequency applications. J Alloy Compd 2011;509:5315–9.
[22] Pathania A, Thakur P, Sharma A, Hsu JH, Thakur Atul. Investigation of iron deficient and manganese doped Ni–Mg nano-ferroxide ceramics. Ceram Int 2015;41:10803–9.
[23] Harris VG, Geiler A, Chen YJ, Yoon SD, Wu MZ, Yang A, et al. J Magn Magn Mater 2009;321:2035–47.
[24] Dalawai SP, Shinde TJ, Gadkari AB, Vasambekar PN. Ni–Zn ferrite thick film gas sensors. J Mater Sci: Mater Electron 2015;26:9016–25.
[25] Sutka Andris, Gross Karlis A. Spinel ferrite oxide semiconductor gas sensors. Sensors Actuat B 2016;222:95–105.
[26] Wang Z, Hua Y, Wang W, Zhang X, Wang B, Tian H, et al. Fast and highly-sensitive hydrogen sensing of Nb_2O_5 nanowires at room temperature. Int J Hydrogen Energy 2012;37:4526–32.
[27] Mondal B, Basumatari B, Das J, Roychaudhury C, Saha H, Mukherjee N. ZnO, SnO2 based composite type gas sensor for selective hydrogen sensing. Sensor Actuat B Chem 2014;194:389–96.
[28] Zhao J, Wang W, Liu Y, Ma J, Li X, Du Y, et al. Ordered mesoporous Pd/SnO_2 synthesized by a nano casting route for high hydrogen sensing performance. Sensor Actuator B Chem 2011;160:604–8.
[29] Zhang C, Wang J, Geng X. Tungsten oxide coatings deposited by plasma spray using powder and solution precursor for detection of nitrogen dioxide gas. J Alloy Compd 2016;668:128–36.
[30] Zhang C, Boudiba A, De Marco P, Snyders R, Olivier M, Debliquy M. Room temperature responses of visible-light illuminated WO_3sensors to NO_2 in sub-ppm range. Sensor Actuat B Chem 2013;181:395–401.
[31] Smith II RD, Liu P, Lee SH, Tracy CE, Pitts JR. Low-cost fiber optic Hydrogen sensors Preprints Fuel Chem Div 2002;47:825–7.
[32] Boudiba A, Roussel P, Zhang C, Olivier M-G, Snyders R, Debliquy M. Sensing mechanism of hydrogen sensors based on palladium-loaded tungsten oxide (Pd–WO_3). Sens Actuat B 2013;187:89–93.
[33] Liu YL, Wang H, Yang Y, Liu ZM, Yang HF, Shen GL, et al. Hydrogen sulfide sensing properties of. $NiFe_2O_4$nanopowder doped with noble metals. Sens Actuat B 2004;102:148–54.
[34] Wang Y, Kong F, Zhu B, Wang S, Wu S, Huang W. Synthesis and characterization of Pd-doped α-Fe_2O_3 $_H2S$ sensor with low power consumption. Mater Sci Eng B 2007;140:98–102.
[35] Sidelev DV, Bleykher GA, Grudinin VA, Krivobokov VP, Bestetti M, Syrtanov MS, et al. Hot target magnetron sputtering for ferromagnetic films deposition. Surf Coat Technol 2018;334:61–70.
[36] Nishikawa H, Umatani S. Effect of ablation laser pulse repetition rate on the surface protrusion density of hydroxyapatite thin films deposited using pulsed laser deposition. Mater Lett 2017;209:330–3.
[37] Hai TH, Van HTB, Phong TC, Abe M. Spinel ferrite thin-film synthesis by spin-spray ferrite plating. Phys B 2003;327:194–7.
[38] Mokurala K, Mallick S, Bhargava P, Siol S, Klein TR, Van Hest Maikel FAM. Influence of dipping cycles on physical, optical, and electrical properties of Cu_2NiSnS_4: Direct solution dip coating for photovoltaic applications. J Alloy Compd 2017;725:510–8.
[39] Lanfredi S, Storti F, Simões LPM, Djurado E, Nobre MAL. Synthesis and structural characterization of calcium titanate by spray pyrolysis method. Mater Lett 2017;201:148–51.

[40] Casciano Paulo NS, Benevides Ramon L, Santana Renato AC, Correia Adriana N, Lima-Neto Pedro de. Factorial design in the electrodeposition of Co-Mo coatings and their evaluations for hydrogen evolution reaction. J Alloy Compd 2017;723:164–71.
[41] Pathania A, Bhardwaj S, Thakur SS, Jean-Luc Mattei P, Queffelec LV, Panina P, et al. Investigation of structural, optical, magnetic and electrical properties of tungsten doped Ni Zn nano-ferrites. Phys B 2018;531:45–50.
[42] Barsan N, Koziej D, Weimar U. Metal oxide-based gas sensor research: How to? Sensor. Actuat. B-Chem. 2007;121:18–35.
[43] Phanichphant S, Liewhiran C, Wetchakun K, Wisitsoraat A, Tuantranont A. Flame-made Nb-doped TiO_2 ethanol and acetone sensors. Sensors 2011;11:472–84.
[44] Takeguchi T, Furukawa S, Inoue M. Hydrogen spillover from NiO to the large surface area CeO_2 ZrO_2 solid solutions and activity of the NiO/CeO_2 ZrO_2 catalysts for partial oxidation of methane. J Catal 2001;202:14–24.
[45] Adams B, Ostrom C, Chen S. Aichengchen. High performance Pd-Based hydrogen spill-over catalysts for hydrogen storage. J Phys Chem C 2010;114:19875–82.
[46] Boudjahem A, Bettahar M. Effect of oxidative pre-treatment on hydrogen spill-over for a Ni/SiO_2 catalyst. J MolCatal AChem. 2017;426:190–7.
[47] Annanouch F, Haddi Z, Ling M, Di Maggio F, Vallejos S, Vilic T, et al. Aerosol-assisted CVD-grown PdOnano particle decorated tungsten oxide nanoneedles extremely sensitive and selective to hydrogen. ACS Appl Mater Interfaces 2016;8:10413–21.
[48] Fan Hong, Shucong Xu, Cao Xianmin, Liu Daoxi, Yin Yaoyu, Hao Haiyong, Wei Dezhou, Shen Yanbai. Ultra-long Z_n2Sn_O4-ZnO microwires based gas sensor for hydrogen detection. Appl Surf Sci 2017;400:440–5.
[49] Sutka A, Mezinskis G, Lusis A, Stingaciu M. Gas sensing properties of Zn-doped p-type nickel ferrite. Sens Actuat B 2012;171–172:354–60.
[50] Ayesh Ahmad I, Mahmoud Saleh T, Ahmad Sadiqa J, Haik Yousef. Novel hydrogen gas sensor based on Pd and SnO2 nanoclusters. Mater Lett 2014;128:354–7.
[51] Maity A, Majumder SB. NO_2 sensing and selectivity characteristics of tungsten oxide thin films. Sens Actuat B 2015;206:423–9.